Chemical Engineering Journal 215–216 (2013) 72–81

Contents lists available at SciVerse ScienceDirect

Chemical Engineering Journal

journal homepage: www.elsevier.com/locate/cej

Polyethersulfone enwrapped graphene oxide porous particles for water treatment

Xiang Zhang [a], Chong Cheng [a], Jing Zhao [a], Lang Ma [a], Shudong Sun [a,*], Changsheng Zhao [a,b,*]

[a] College of Polymer Science and Engineering, State Key Laboratory of Polymer Materials Engineering, Sichuan University, Chengdu 610065, China
[b] National Engineering Research Center for Biomaterials, Sichuan University, Chengdu 610064, China

HIGHLIGHTS

- PES enwrapped GO porous particles were prepared by a liquid–liquid phase separation technique.
- This strategy made GO easily controlled and withdrew during the adsorption process.
- The PES/GO porous particles showed good selective adsorbability to cationic dyes.

ARTICLE INFO

Article history:
Received 4 August 2012
Received in revised form 2 November 2012
Accepted 3 November 2012
Available online 9 November 2012

Keywords:
Graphene oxide
Polyethersulfone
Methylene blue
Adsorption
Wastewater

ABSTRACT

Recent studies showed that graphene oxide (GO) presented high adsorption capacities to various water contaminants. However, the high water dispersibility of GO restricted its practical applications in wastewater treatment since ultrahigh centrifugation was necessary after the adsorption process. In this study, a facile method was presented by enwrapping GO in porous particles to remove dyes and other pollutions from wastewater. Polyethersulfone (PES) was chosen as the matrix to enwrap GO through a liquid–liquid phase separation process, the PES/GO porous particles showed a dense skin layer and a porous structures of the inside. Methylene blue (MB), a cationic dye, was chosen as the adsorbate to investigate the adsorption capability, kinetics and isotherms of the prepared particles, and the particles displayed an adsorption capacity up to 62.5 mg/g for MB dye. Meanwhile, the effect of contacting time, initial concentration, temperature, and pH value on the adsorption capacity was studied. The experimental data of MB adsorption fitted the pseudo-second-order kinetic model and the Langmuir isotherm very well, and the adsorption process was controlled by the intraparticle diffusion. Moreover, the results indicated that the PES/GO porous particles showed good selective adsorbability to cationic dyes, such as MB and methyl violet.

1. Introduction

Nowadays, the widespread use of chemical compounds around the world has led to serious water pollution, especially the industrial dyes, which may lead to retention toxicosis, lethal poison and carcinogenic contact to human beings and animals even at ultralow concentrations [1]. As a result, the removal of dyes from industrial wastewater, such as methylene blue (MB), has become a critical issue [2]. Various approaches to remove dyes from water have been explored and developed [3,4]. Among them, adsorption has gained importance as a purification and separation technique in industrial scales and becomes an attractive option for industrial water treatment, especially the removal of organic compounds that are chemically and biologically stable [5,6]. Till now, it has been reported that clays [7–10], hydrophobic porous polymer [11] and carbon-based materials [12] could selectively remove water pollutants. Among these materials mentioned above, carbon-based materials are the most promising adsorbents due to their high-specific surface area, high chemical and mechanical stabilities [13]. Recently, carbon-based nanomaterials, such as graphite [14], fullerene [15], and carbon nanotube (CNT) [16], which play a major role in the fields of electronics and sensors, demonstrated their capability as an effective sorbent for inorganic and organic contaminants. However, most of these engineered carbon materials require high-cost fabrication process [17].

Graphene oxide (GO), which was produced from graphite using various chemical oxidation routes, is one of the most important derivatives of graphene. It is characterized by a layered structure with oxygen functional groups bearing on the basal planes and edges [18], which endow it an ultra-large specific surface area and negative charge surface. As a result, GO may have outstanding adsorption effect of cationic compounds. Moreover, GO sheet can be produced in a large scale by exfoliating from the cheap graphite

* Corresponding authors. Address: College of Polymer Science and Engineering, State Key Laboratory of Polymer Materials Engineering, Sichuan University, Chengdu 610065, China. Tel.: +86 28 85400453; fax: +86 28 85405402.
E-mail addresses: stephen9988@126.com (S. Sun), zhaochsh70@scu.edu.cn (C. Zhao).

1385-8947/$ - see front matter © 2012 Elsevier B.V. All rights reserved.
http://dx.doi.org/10.1016/j.cej.2012.11.009

[19]. These factors provide GO with ideal characteristics as an excellent adsorbent. Zhang et al. [20] studied the MB adsorption by aqueous dispersed single layer GO, and the adsorption capability was quite high. However, since GO was nano-materials and presented high dispersibility in aqueous solution [21], the practical application and collection of GO sheet become difficult after adsorption process, meanwhile, the unprecipitated GO may lead to potential nano-toxicity to aquatic creatures. These problems restrict the practical applications of GO as adsorbents on a large scale. Therefore, it still remains as a challenge to immobilize GO into macroscopical and practical material. To overcome this problem, various methods have been investigated, such as blending GO with polystyrene [22] and generating GO aerogel [17]. However, up to now, there is no preferable method to immobilize GO well and also exhibit satisfactory adsorption capacity.

In this paper, polyethersulfone (PES) was chosen as a polymeric matrix to prepare PES/GO porous particles. As a well-known polymeric material, PES can be prepared into porous particles with fine surface morphology by means of a facile liquid–liquid phase separation technique [23]; the porosity of the particles can reach 80%, and the particles showed outstanding oxidative, thermal, and hydrolytic stabilities as well as good mechanical properties [24,25]. Meanwhile, appropriate concentration of GO can disperse well in PES/N, N-dimethyl acetamide (DMAC) solution homogeneously. Therefore, it is reasonable to predict that, by blending GO sheet with PES solution and the subsequent phase inversion process, the obtained PES/GO particles may provide a porous and stable support to immobilize GO and achieve a high adsorption capacity to satisfy practical application in wastewater treatment. Thus, in this study, PES/GO porous particles were prepared first, and then the inner structure of the particles was characterized by scanning electron microscopy (SEM). Methylene blue (MB), a cationic dye, was chosen as the adsorbate to investigate the adsorption capability, kinetics and isotherms of the prepared particles. To further investigate the selective adsorbability of the particles, different pollutants, including some dyes and endocrine disruptors with different polarities and solubilities in water such as methyl violet (MV, cation), Congo red (CR, anion), bisphenol A (BPA, nonionic), and biphenyl (BP, nonionic) were tested.

2. Materials and methods

2.1. Materials

Graphite flakes were purchased from Sigma–Aldrich. The substrates, including mica and silicon wafers were all commercially available. Polyethersulfone (PES, Ultrason E6020P, and CAS No. 25608-63-3) was purchased from BASF chemical company (Germany). Dialysis membranes (MWCO = 8000–14,000 Da) were obtained from Solarbio (Canada). Unless otherwise stated, other reagents were obtained from Aladdin reagent Co. Ltd. (China) with analytical grade and used as received. All aqueous solutions were prepared with de-ionized water (DI water).

2.2. Preparation and characterization of GO

Graphene oxide (GO) was prepared from natural graphite flakes by a modified Hummers method [26]. Briefly, 5 g graphite and 3.75 g $NaNO_3$ were placed in a flask. Then, 150 ml H_2SO_4 was added with stirring in an ice–water bath, and 20 g $KMnO_4$ was slowly added for over 1 h. The mixture was stirred in the ice water bath for 2 h, following by a vigorously stirring for 3 days at room temperature. Then, the mixture was diluted with DI water (500 ml) slowly, and the excessive $KMnO_4$ was decomposed by H_2O_2 (30 wt.%, 15 ml). The insoluble precipitations were removed by centrifugation. The resulted GO solution was filtered and washed with HCl (10 wt.%, 1 l) and DI water for several times to remove the metal ions. The pristine brown GO solution was dialyzed with DI water for 1 week before use to remove any residual salts and acids.

The prepared GO samples were characterized using various techniques such as atomic force microscopy (AFM), Fourier transform infrared spectroscopy analysis (FTIR), scanning electronic microscope (SEM) and zeta potential measurements. AFM images were taken on a Multi-Mode Nanoscope V scanning probe microscopy (SPM) system (Vecco Instruments Co., USA). The commercially available AFM cantilever tips with a force constant of ~48 N/m and resonance vibration frequency of ~330 kHz were used. The scanning rate was set at 0.4–0.8 Hz. The samples for AFM were prepared by dropping aqueous GO dispersion (~0.01 mg/mL and sonicated for 5 min with an ultrasonic bath cleaner) on freshly cleaved mica surface and dried under vacuum at 60 °C. FTIR patterns were obtained using a FTIR spectrometer (Nicolet 560, USA). The samples for FTIR measurement were prepared by grinding the dried powder with KBr together, and then pressed into a pellet for the FTIR characterization. SEM images were obtained by drop-casting the aqueous GO solution on the silicon wafer. A scanning electron microscope (FEI Sirion-200, USA) was used for the surface morphology observation. Zeta potential measurement of the aqueous dispersion of GO (~0.01 mg/mL) was performed in DI water using Zetasizer ZS90 (Malvern Instruments Ltd., UK). Each measurement was repeated at least three times.

2.3. Preparation and characterization of PES/GO porous particles

The prepared GO suspension was centrifuged firstly, and then the concentrated GO suspension was freeze-dried for 24 h to remove water. Then, a required amount of the dry GO was dispersed in DMAC, and ultrasound for 30 min to get a homogeneous mixture. A required amount of PES was added in, which was then dissolved and mixed with GO by magnetic stirring apparatus for 12 h. Before the fabrication of particles, the mixture was treated with sonication for 10 min.

The PES/GO porous particles were prepared by a liquid–liquid phase separation technique. This technique was described in detail in our earlier report [23]. The schematic illustration of the preparing process is outlined in Fig. 1. The resultant solution prepared above was dropped into DI water with a 0.7-mm diameter syringe needle at room temperature. The DI water was stirred at about 300 rpm by magnetic stirring apparatus. The injection speed was controlled at 60–100 drops/min. The tip of the syringe needle was 5–8 cm above the surface of the water. In order to get regular and smooth particles, the concentration of the PES solution was

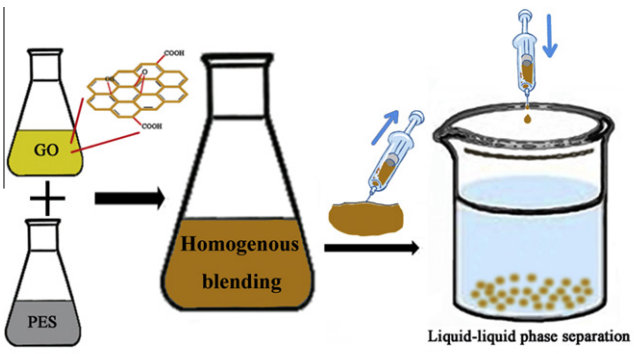

Fig. 1. The schematic illustration for preparing PES/GO particles.

controlled at 12 wt.%. For the sake of comparison, a series of PES/GO porous particles with different mass ratios of GO to the PES were prepared, which were controlled at 12%, 9%, 6%, 3%, 0%, and named as PES/GO-4, PES/GO-3, PES/GO-2, PES/GO-1 and PES/GO-0, respectively. The particles were then placed in DI water for 24 h to remove residual DMAC.

The prepared particles were characterized by scanning electron microscopy, BET-N_2 adsorption/desorption experiments and zeta potential measurements. For the SEM (JSM-7500F, JEOL) observation, the particles were dried in an oven to constant weight, and then cut by a single-edged razor blade after immersing into liquid nitrogen. Thereafter, the prepared samples were attached to the sample supports and coated with a gold layer before observation. BET–N_2 adsorption/desorption experiments were carried out manometrically at −196 °C using an auto-porosity analyzer (Micromeritics TriStar 3000, USA). All the particles were degassed overnight at 160 °C, prior to the adsorption experiments. The BET surface area and pore volume were obtained by applying the BET equation and $p/p_0 = 0.99$ to the adsorption data, respectively. The pore size distribution was obtained by the BJH method. Zeta potential measurement of the particles was performed by using Zetasizer ZS90 (Malvern Instruments Ltd., UK). PES/GO-0, PES/GO-1 and PES/GO-3 were chosen for this test. About 10 g of the particle was dried at 60 °C over night, triturated into powder, and then dispersed into DI water. Each measurement was repeated at least three times.

2.4. Adsorption experiments

The adsorption of MB onto GO aqueous solution was carried out in water at room temperature and pH 7. In general, 5 ml of 1 mg/l GO aqueous solution was added to 20 ml of MB solution (0.1–2 mmol/l) in conical flasks, after stirring by a magnetic stirrer for 30 min to reach equilibrium, GO was centrifuged at 12,000 r/min for 10 min from MB solution and the concentrations were determined with the UV–vis spectrophotometer 756PC at the wavelength of 631 nm.

For the adsorption experiments of the particles, in order to discuss the effect of the GO amounts in the particles on the adsorption, 20 particles (about 0.025 g in dry weight) were applied in 20 ml of 150 μmol/l MB solution in conical flasks at the temperature of 30 ± 1 °C with the stirring speed of 100 rpm, and the pH value of the solution was 7. The MB concentrations were determined at different time intervals with the UV–vis spectrophotometer 756PC at the wavelength of 631 nm [27]. The data were also used for adsorption kinetics study. To study the effect of the initial concentrations, PES/GO-1, PES/GO-2, PES/GO-3 and PES/GO-4 particles were applied to 20 ml MB solutions with the initial concentrations were 50, 100, 150, 200, and 250 μmol/l, respectively. The concentrations were also determined at different time intervals and the data were also used for analyzing adsorption isotherm.

PES/GO-3 particles were chosen optionally for discussing the effect of temperature and pH values. The adsorption process was carried out at 15, 30, 45 and 60 °C, respectively; other conditions (amount of particles, volume of solution, pH value and stirring speed) were the same as above and the concentration of MB solution was 150 μmol/l. To study the effect of pH value, the pH values of MB solutions (150 μmol/l) were controlled at 3, 5, 7, 9 and 11 by adding hydrochloric acid or sodium hydroxide solutions, other conditions (amount of particles, volume of solution and stirring speed) were unchanged, and the experimental temperature was 30 ± 1 °C. The concentrations of these solutions were determined when equilibrium was reached.

The desorption experiments were carried out as follows: after adsorption, the PES/GO-3 particles were applied into 20, 50 and 100 ml DI water with 0.05 M hydrochloric acid, respectively, and stirred using a magnetic stirring apparatus. After 24 h, the concentrations of the MB in the hydrochloric acid solutions were determined, and the particles were moved to the fresh hydrochloric acid solutions for continued desorption. This process was repeated for three times. In each time, the desorption ratio (R_d) was obtained as:

$$R_d = \frac{n_d}{n_a} \times 100\% \quad (1)$$

where n_d is the amount of the MB desorbed to the solution, n_a is the amount of the MB adsorbed by the particles, which was calculated from the adsorption experiments. The total desorption ratios were the sum of the R_d for the three repeating times.

At last, the selective adsorption capabilities of the particles to MV, CR, BPA and BP were tested. The PES/GO-3 particles were applied in 20 ml of 150 μmol/l solutions in conical flasks at 30 ± 1 °C with stirring at 100 rpm, and the pH value was 7. The concentrations of the solutions were determined after 12 h. The removal ratio (R) of the reagent was determined by the sorption method using the following equation:

$$R = \frac{C_0 - C_t}{C_0} \times 100\% \quad (2)$$

where C_0 is the initial concentration of the solution (μmol/l); C_t is the concentration at the time t (μmol/l).

3. Results and discussion

3.1. Characterization of GO

AFM image (SI Fig. S1a) and SEM image (SI Fig. S1b) of the prepared GO demonstrated that the GO sheets were two-dimensional single layer structure, the average thickness of each single layer was about 1.1 nm. The infrared spectrum of prepared GO (SI Fig. S1c) indicated that hydroxyl groups, epoxy groups and carboxyl groups were presented on the GO sheet, and because of that, the surface of GO sheet showed negative charges, the Zeta potential of the GO sheet was about −41 mV.

3.2. Characterization of PES/GO porous particles

A liquid–liquid phase separation technique was employed for the preparation of the particles. As the dispersibility of GO in DMAC was limited, in order to avoid the blocking of syringe needle due to the overlapping and agglomeration between the GO sheets, the concentration of GO must be controlled. Many attempts showed that the particles could be prepared successfully by the liquid–liquid phase separation technique at the mass ratio of GO to PES lower than 12%.

The SEM pictures of PES/GO-0, PES/GO-1 and PES/GO-4 are shown in Fig. 2. Each kind of the particles has been taken in three forms: the panorama of cross-section, the skin layer morphologies and the partial regions of the cross-sections in high magnification. For PES/GO-0, the "dense skin layer" [28] and the pores with the finger-like structure were clearly observed (see Fig. 2a1), and the pore size gradually increased from the outer surface to the internal region of the particle. With the increased of the GO amount in the particles, the skin layer could also be observed, and the finger-like structure disappeared and porous structure became compact gradually (see Fig. 2b1 and c1). The beads in the images which were magnified 15,000 times (see Fig. 2a3–c3) were formed by phase separation of PES during the liquid–liquid phase separation process, it could be observed in each kind of particles. GO, which could be observed in the 15,000 times magnifying pictures of PES/GO-1 and PES/GO-4 (see Fig. 2b3 and c3, the red arrows), was the gossamer substance which looked like surface wrapping. This morphology of GO had also been observed in other researches [29,30].

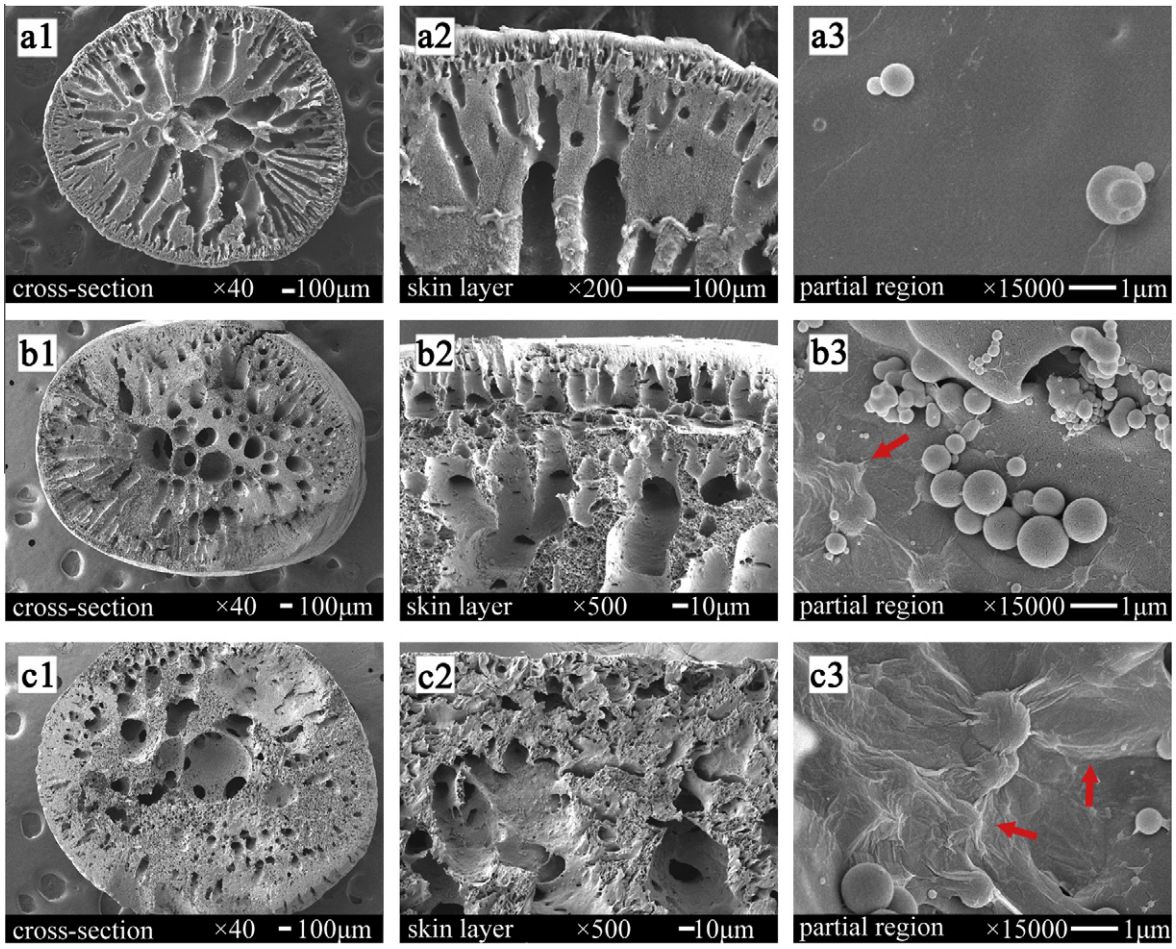

Fig. 2. The SEM images for the cross-sections, skin layers and partial regions in high magnification for PES/GO-0 (a1, a2, and a3), PES/GO-1 (b1, b2, and b3) and PES/GO-4 (c1, c2, and c3). In b3 and c3, GO is pointed by the red arrows.

Table 1 shows the physical properties of the particles. It can be seen that the values of S_{BET}, volume of mesopore (V_{meso}) and BJH pore sizes of PES/GO-0, PES/GO-1 and PES/GO-3 are very close. The mesopore size distributions are shown in Fig. 3. The results indicated that the blending of GO had barely effect on the mesopore size distribution of the PES particles; the PES/GO-0 and PES/GO-1 had almost the same pore size distribution, and a slight decrease could be observed in PES/GO-3. Most of the pore sizes were less than 5 nm, revealing a lot of micropores existed in the particles. Considering that the N_2 adsorption only provided the information of mesopores and many macropores could be observed in the SEM images, a calculating method of the porosity and total pore volume (V_{tot}) for the particles (see SI) was used. The results are shown in Table 1, and the values of the porosity and V_{tot} for different particles are also similar. The Zeta potentials for PES/GO-1 and PES/GO-3 were increased (as shown in Table 1), due to the increase of the concentration of the GO in the particles.

The SEM images and the data in Table 1 indicated that the internal macrostructure of the hybrid particles were changed after blending GO, however, the surfaces, mesopore sizes and distribution, porosity and total volume were barely changed. The porous

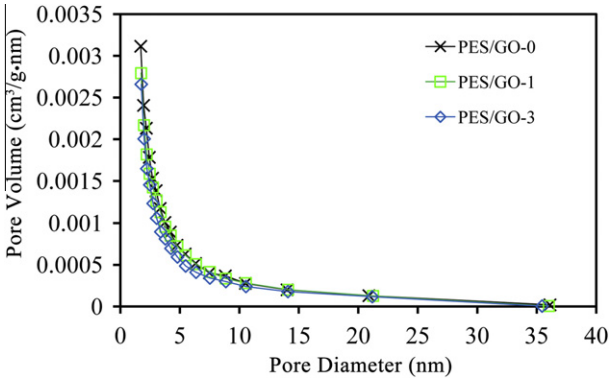

Fig. 3. The mesopore size distribution of particles.

Table 1
Physical properties of particles.

	S_{BET} (m^2/g)	V_{meso} (cm^3/g)	BJH pore size (nm)	Porosity (%)	V_{tot} (cm^3/g)	Zeta potential (mV)
PES/GO-0	25.67	0.0148	5.59	86.48	4.49	−6.3 ± 2.0
PES/GO-1	23.09	0.0161	6.49	86.21	4.26	−12.3 ± 4.0
PES/GO-3	24.98	0.0142	6.53	85.65	4.32	−29.9 ± 4.0

structure and dense skin layer could not only maintain the high adsorption capacity of GO, but also immobilize the highly dispersed GO and prevented the elution of nano-sized GO from the porous polymer matrix.

3.3. Adsorption of MB by the particles

3.3.1. Effect of GO concentration and MB initial concentration

The MB adsorbed amounts per unit mass of the particles are shown in Fig. 4a, the adsorbed amount increased with the increase of the GO mass ratios in the particles. All the adsorption processes reached equilibrium after about 60 h, the long equilibrium time might be caused by the porous structure of the particles: the interior micropores were abundant, in which the diffusion of the adsorbates would take a long time. The adsorbed amount of PES/GO-0 was very low, so the adsorption of MB was largely attributed to the GO sheets, while PES mainly functioned as a matrix to embed GO. The adsorbed amounts of PES/GO-1, PES/GO-2, PES/GO-3 and PES/GO-4 were 29.01, 35.70, 40.41 and 42.81 mg/g, respectively. The data also indicated that the increased mass of GO and the increased adsorbed amount did not fit linearity; when the GO mass increased, the utilization efficacy of GO became lower. These results might be attributed to the dispersity of GO sheets, the possibility of overlapping and agglomeration between GO sheets might increase significantly at high GO concentrations.

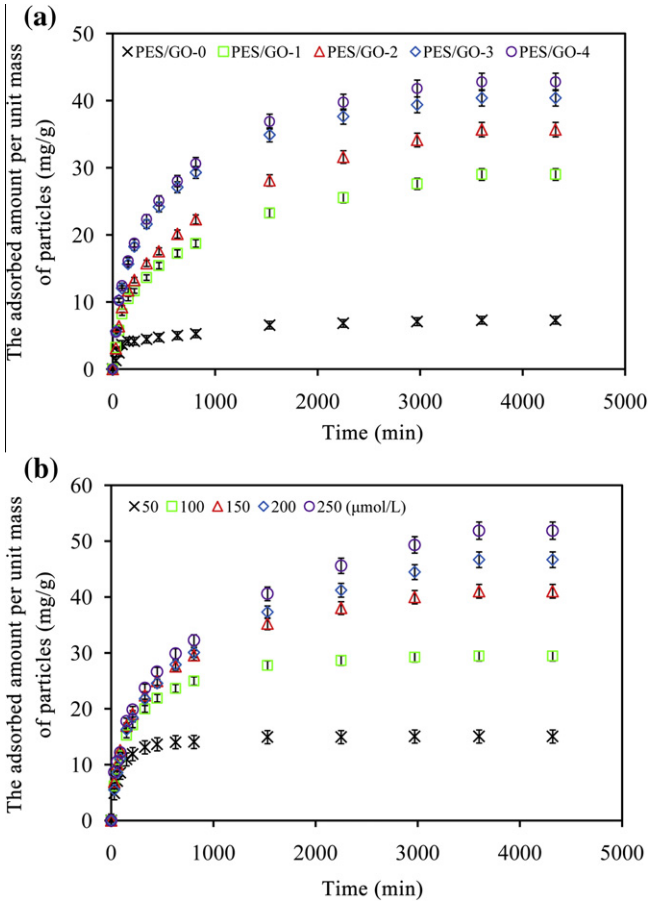

Fig. 4. The adsorbed amounts per unit mass for PES/GO-0, PES/GO-1, PES/GO-2, PES/GO-3 and PES/GO-4. 20 particles are applied in 20 ml of 150 μmol/l MB solution (a); the adsorbed amounts per unit mass of PES/GO-3 at various initial concentrations. 20 PES/GO-3 particles are applied in 20 ml MB solution (b). The adsorption experiment are carried out at 30 ± 1 °C with 100 rpm stirring speed, the pH value of the solution is 7. Data are expressed as the mean ± S.D. of three independent measurements.

The effect of initial concentration on the adsorbed MB amount to the PES/GO particles was investigated. The adsorbed amounts of PES/GO-3 at various initial concentrations are shown in Fig. 4b. With the increase of the initial concentration, the adsorbed amounts of PES/GO-3 increased. The maximum adsorbed amounts of MB at the concentrations of 50, 100, 150, 200, 250 μmol/l, were 15.04, 29.46, 41.04, 46.67, and 51.88 mg/g, respectively. The increase of the maximum adsorbed amount could be attributed to the increased contacting probability between the MB molecules and the adsorbing sites in the particles. Moreover, high concentration could accelerate the diffusion of the MB molecules into the particles.

3.3.2. Effect of pH and temperature

The adsorption mechanism of MB onto GO could be attributed to electrostatic attraction [31], the change of pH values of the solution could change the surface charge of GO, so it might have a significant effect on the adsorbed amount of MB. Fig. 5a shows the relationship between the pH values of the solutions and the adsorbed amounts. It is found that the adsorbed amounts of PES/GO-3 and PES/GO-1 increased with the increase of the pH values of the solutions, while it did not change for PES/GO-0. Meanwhile, with the increase of pH values, the increase of adsorbed amount of PES/GO-1 was less than PES/GO-3.

The results could be prejudged: at low pH values, a relatively high concentration of H^+, which competed strongly with MB cations for adsorption sites, would be available to protonate hydroxyl groups of the GO surfaces to form $-OH_2^+$ groups. Furthermore, the protonation of hydroxyl groups would lead to electrostatic repulsion, which would restrict MB cations to come into close contact with the adsorbent surface [32]. These factors reduced the adsorbed amounts of the particles. When the pH value increased, the hydroxyl groups would dissociate and form $-O^-$ groups, which might enhance the electrostatic attraction between the adsorbent surface and MB cations. The number of H^+ also decreased at higher pH values, the competition between H^+ and MB cations became less significant. Consequently, the adsorbed amount of the particles increased. The effect of pH values on the adsorbed amount for PES/GO-1 was less than for PES/GO-3, this might because the amount of GO in PES/GO-1 was less than PES/GO-3, the adsorption sites which would be influenced by pH were fewer, as a result, the changing of the adsorbed amounts of PES/GO-1 was smaller. As a hydrophobic material, PES had not those sites which could ionize in different pH values, and the electrostatic interaction could not occur between PES and MB, so the adsorbed amounts of PES/GO-0 had no change with the changing of pH.

The effect of temperature on the adsorbed amounts for PES/GO-3, PES/GO-1 and PES/GO-0 is shown in Fig. 5b. The results indicated that with the increase of temperature, the adsorbed amount of PES/GO-3 and PES/GO-1 increased, indicating an endothermic nature of the adsorption process, while the adsorbed amount of PES/GO-0 had no change. When the temperature increased, the ionization of the hydroxyl became strong, resulting in the increase of the adsorption sites, so the adsorbed amounts to the PES/GO-3 and PES/GO-1 increased. By changing the temperature, the increase of the adsorbed amount to the PES/GO-1 became smaller and no change for PES/GO-0, and the reason was the same as those had been explained for the relation between the adsorbed amounts and different pH values.

3.4. Desorption of MB from the particles

The desorption experiment was carried out in 20 ml, 50 ml and 100 ml aqueous solutions with 0.05 mol hydrochloric acid, respectively. In each acidic solution, PES/GO-3 was used for the desorption after the adsorption experiments. As the rate of desorption

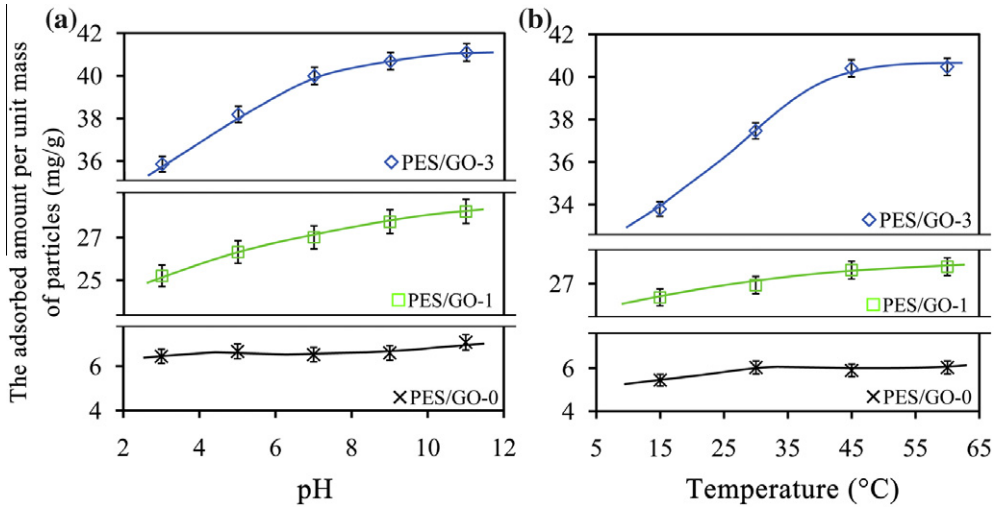

Fig. 5. Effect of pH value on the MB adsorption for PES/GO-0, PES/GO-1 and PES/GO-3 particles. 20 particles are applied in 20 ml MB solutions at 30 ± 1 °C with 100 rpm stirring speed, the values of pH of MB solutions are 3, 5, 7, 9 and 11, respectively (a). Effect of temperature on MB adsorbed amounts by PES/GO-0, PES/GO-1 and PES/GO-3. 20 particles are applied in 20 ml MB solutions with 100 rpm stirring speed, the value of pH is 7, and the temperature of the solutions are 15, 30, 45 and 60 °C, respectively (b). Data are expressed as the mean ± S.D. of three independent measurements.

was slow, the acidic solution was replaced with fresh one every 24 h. The desorption ratios for different repeating times and different amounts of solutions are shown in Fig. 6. As shown in the figure, the desorption efficiency was affected by the amount of the solutions. The total desorption ratio was only 73.2% in 20 ml acidic aqueous solution even the solution was replaced for three times, however, it could reach to 95.0% and 97.5% in the 50 ml and 100 ml acidic aqueous solutions, respectively. The results indicated that the PES/GO particles could be reused.

3.5. Adsorption kinetics study

In this study, three kinetic models were used to test the experimental data, i.e. the pseudo-first-order equation, the pseudo-second-order equation and the intraparticle diffusion equation.

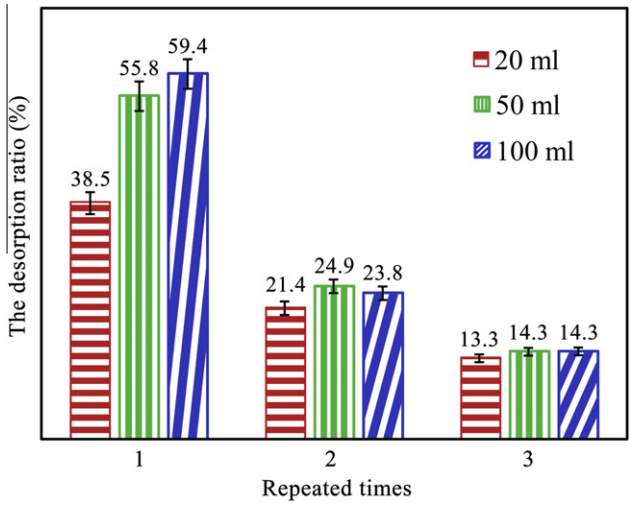

Fig. 6. The desorption ratios of the adsorbed MB in acidic aqueous solutions. 20 PES/GO-3 particles which reached adsorption equilibrium were applied into 20, 50 and 100 ml DI water with 0.05 M hydrochloric acid, respectively, and stirred using a magnetic stirring apparatus. After 24 h, the particles were removed and applied to fresh hydrochloric acid solutions. This process was repeated three times. Data are expressed as the mean ± S.D. of three independent measurements.

3.5.1. The pseudo-first-order and pseudo-second-order kinetic model

The pseudo-first-order kinetic model is more suitable for low concentration of solute [33]. The fitting result indicated that the experimental data did not agree well with this model (see SI). The pseudo-second-order equation is dependent on the amount of the solute adsorbed on the surface of adsorbent and the amount adsorbed at equilibrium [33]. It can be represented in the following form [34]:

$$\frac{t}{q_t} = \frac{1}{k_2 q_e^2} + \frac{t}{q_e} \tag{3}$$

where k_2 is the rate constant of pseudo-second-order equation, q_t, q_e, and t have the same meaning as that in pseudo-first-order equation. From the slope and intercept of the plot of t/q_t versus t which are shown in Fig. 7a, the rate constant (k_2) and the equilibrium adsorption capacity (q_e) can be obtained. As seen in Table 2, all the correlation coefficients (r^2) were higher than 0.99, which mean that the adsorption of MB by the PES/GO particles fitted the pseudo-second-order model very well. The calculated values of q_e were smaller than the experimental ones; however, the calculated q_e values for PES/GO-3 and PES/GO-4 were closer to the experimental values than those in the pseudo-first-order model.

3.5.2. The intraparticle diffusion model

As the diffusion mechanism during the adsorption cannot be identified by means of the pseudo-first-order and the pseudo-second-order equations, the intraparticle diffusion [35] model was used. The intraparticle diffusion equation can be written in the following form:

$$q_t = k_p t^{1/2} + C \tag{4}$$

where k_p is the rate constant of intraparticle diffusion model, C is a constant for any experiment (mg/g), q_t has the same meaning as that in Eq. (4). By plotting q_t versus $t^{1/2}$ the curves with three steps were obtained. As seen in Fig. 7b, the slope of the linear part of each curve could give the rate constants, from the extrapolation of the first step in the curves to the time axis, the intercepts C could be obtained. As seen in Table 3, the intercepts were negative, which indicated that the boundary layer in the particles impeded the intraparticle diffusion, the adsorption process was rather complex; the intraparticle diffusion was not the only rate-limiting step, most

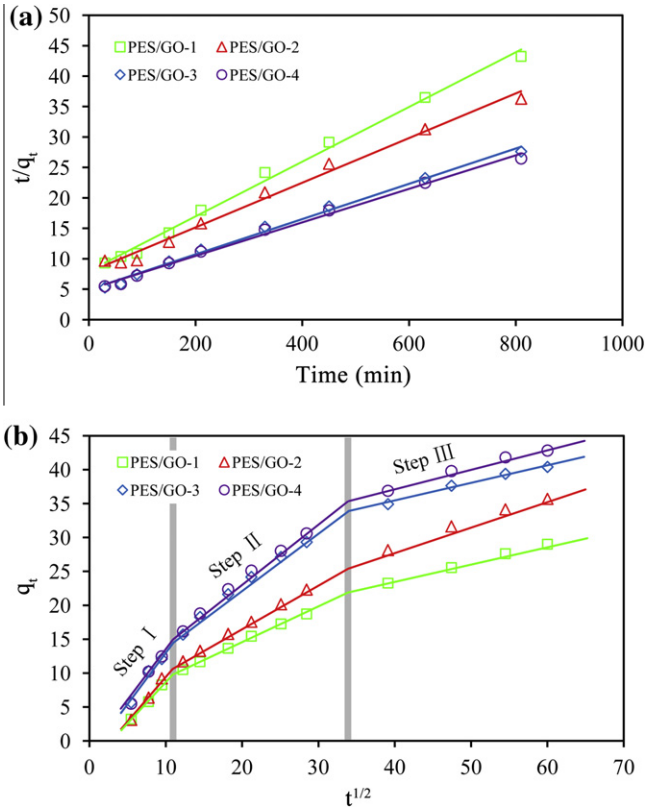

Fig. 7. Application of the pseudo-second-order adsorption model: (a) the intraparticle diffusion model; and (b) for the adsorption of MB onto PES/GO particles.

Table 2
The parameters of pseudo-second-order model for the adsorption of MB by the particles.

Particles	k_2 (g/mg min)	$q_{e(cal)}$ (mg/g)	r^2
PES/GO-1	2.42×10^{-4}	22.73	0.995
PES/GO-2	1.66×10^{-4}	27.78	0.990
PES/GO-3	1.71×10^{-4}	34.48	0.994
PES/GO-4	1.47×10^{-4}	37.04	0.994

of the correlation coefficients (r^2) were higher than 0.99, which mean that the adsorption of MB by the PES/GO particles fitted this model very well. The three slopes in each curve indicated that there were at least three diffusion forms during the adsorption process: the external surface adsorption or diffusion in macro-pores occurred at the first step; the second step, which was controlled by intraparticle diffusion, was the gradual adsorption step; the third step was the final equilibrium step, for which the adsorbent molecules moved slowly from larger pores to micropores and caused a slow adsorption rate. The interpretation of this phenomenon had also been reported by other authors [36,37].

3.6. Adsorption isotherm

Adsorption properties and equilibrium data, commonly known as the adsorption isotherms, described how pollutants interact with sorbent materials, are critical in optimizing the use of adsorbents. In order to optimize the design of an adsorption system to remove dye from solutions, it is important to establish the most appropriate correlation for the equilibrium curve [38]. Herein, Langmuir and Frenundlich adsorption isotherms were used to investigate the adsorption process.

3.6.1. Langmuir isotherm

The Langmuir adsorption isotherm has been successfully applied to many pollutants adsorption process and has been the most widely used adsorption isotherm for the adsorption of solute from a liquid solution [39], it was deduced by several hypothesizes: monolayer adsorption; dynamic balance; no interaction between adsorbate molecules; every adsorption sites have the same adsorptive power. The Langmuir equation is obtained as:

$$\frac{C_e}{q_e} = \frac{1}{q_{\max} k_L} + \frac{C_e}{q_{\max}} \tag{5}$$

where q_e is the mass of the MB adsorbed by the unit mass after the adsorption reaches equilibrium (mg/g); C_e is the equilibrium concentration of the MB (mg/l); $q_{\max}$ is the maximal adsorbed amount of the particles (mg/g); k_L is the Langmuir adsorption constant. A plot of C_e/q_e versus C_e shown in Fig. 8a give a straight line with the slope of $1/q_{\max}$ and the intercept $C_e/(q_{\max})$; the parameters are shown in Table 4. All the values of the correlation coefficient (r^2) for the Langmuir equation were higher than 0.98, which indicated that the adsorption of MB on the PES/GO particles followed the Langmuir adsorption isotherm, and the adsorption process was monolayer adsorption. The maximum adsorption amounts on the PES/GO particles were increased with the increase of the mass percentage of GO; however, the amount for PES/GO-3 was higher than that for PES/GO-4. The results indicated that though PES/GO-4 particles had the highest mass percentage of GO, PES/GO-3 had the maximum adsorption amount; this was caused by the lower dispersity of GO at relatively higher concentration, and the decreased utilization efficacy of GO. PES/GO-3 with the 9% mass ratio of GO to PES might be the best collocation in this study.

3.6.2. Freundlich isotherm

The Freundlich isotherm [24] is an empirical equation, and its initial form is:

$$q_e = k_F C_e^{1/n} \tag{6}$$

where k_F is the Freundlich isotherm constant; q_e and C_e has the same meaning as that in Eq. (6); $1/n$ is the influence coefficient of solution concentration to the equilibrium adsorbed amount. The linear form of the Freundlich isotherm equation can be obtained by taking the logarithm of the following equation:

$$\ln q_e = k_F + (1/n) \ln C_e \tag{7}$$

Table 3
The parameters of intraparticle diffusion model for the adsorption of MB by the particles.

Particles	C (mg/g)	Step I		Step II		Step III	
		k_1 (mg/g min$^{1/2}$)	r_1^2	k_2 (mg/g min$^{1/2}$)	r_2^2	k_3 (mg/g min$^{1/2}$)	r_3^2
PES/GO-1	−3.72	1.25	0.995	0.51	0.997	0.28	0.999
PES/GO-2	−5.30	1.52	0.998	0.65	0.999	0.36	0.993
PES/GO-3	−2.91	1.62	0.969	0.84	0.992	0.26	0.986
PES/GO-4	−3.92	1.76	0.983	0.88	0.994	0.29	0.985

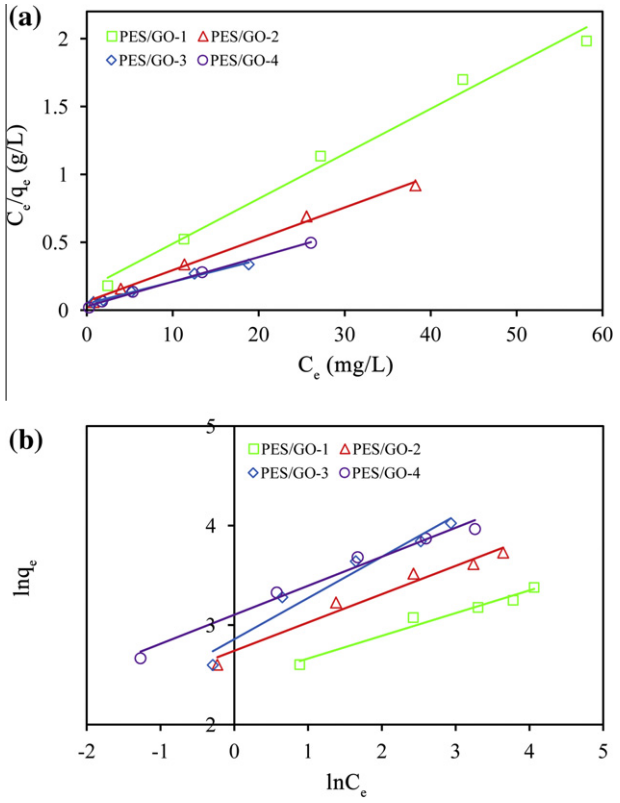

Fig. 8. Application of Langmuir adsorption isotherm (a); and Freundlich adsorption isotherm (b) of MB onto PES/GO particles.

Table 4
The parameters of Langmuir and Freundlich isotherm for the adsorption of MB by the particles.

Particles	Langmuir			Freundlich		
	q_{max} (mg/g)	k_L (l/mg)	r_L^2	n	k_F (l/g)	r_F^2
PES/GO-1	30.30	0.21	0.988	4.39	11.42	0.967
PES/GO-2	43.48	0.36	0.994	3.52	15.50	0.967
PES/GO-3	62.50	0.33	0.989	2.42	17.43	0.953
PES/GO-4	55.56	0.64	0.997	3.44	22.26	0.978

A linear plot was obtained when $\ln q_e$ was plotted against $\ln C_e$, as shown in Fig. 8b, and then the parameters (as shown in Table 4) were obtained. It indicated that the adsorption process also fitted this model but the linear correlation coefficients were smaller than those for the Langmuir model. All the values of n were above to unity, which indicated that the adsorption process was a favorable physical process.

3.7. Comparison of adsorption capacity between GO in aqueous solution and in particles

Enwrapping GO with PES achieved good effect of the fixed GO and made GO easily separated from aqueous solution; however, the adsorption capacity might be influenced after the blending process. In order to discuss this effect, the adsorbed amount of MB by GO aqueous solution was investigated (see SI), and the adsorption

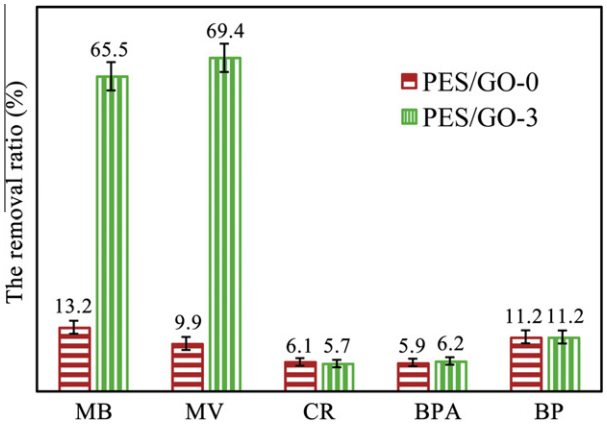

Fig. 9. The removal ratios for different pollutants by PES/GO-0 and PES/GO-3 after 12 h. 20 particles are applied in 20 ml of 150 μmol/l pollutant solutions at 30 ± 1 °C with 100 rpm stirring speed, the pH value of the solution is 7. Data are expressed as the mean ± S.D. of three independent measurements.

capacity of the unit mass of GO in the particles was calculated by the simple formula:

$$q_{GO} = \frac{q_{max}}{R} \quad (8)$$

where q_{GO} is the adsorbed amount of pure GO in each particles (mg/g); q_{max}, which was obtained from the calculation of Langmuir model, is the maximal adsorbed amount of the particles (mg/g); R is the mass ratio of GO to PES for the particle (%). As shown in Table 5, the results indicated that the pure GO had the highest adsorption capacity; after blending with PES, the adsorption capacity decreased; and with the increase of the GO amounts in the particles, the adsorption capacity decreased gradually. These might be caused by the coverage of the adsorption sites by PES and the agglomeration between GO sheets; and this effect might increase when the GO concentration was increased. The adsorbed MB amounts by various materials had discussed by some researches: the adsorbed amount of MB in sepiolite was about 100 mg/g [27]; the adsorbed amount of GO aerogel was about 450 mg/g [17]; activate carbon adsorption capability of MB was about 300–500 mg/g [40,13]. By contrast, GO could still display outstanding adsorption capacity after the blending process.

3.8. Adsorption of different kinds of water pollutants by the particles

Besides the porous structure interiorly, the special adsorption capability of PES/GO particles could be attributed to the negative charge in the surface of the GO sheet, which conferred it high selective adsorbability to cationic dyes. To further confirm the adsorption character of the particles, different pollutants, including cationic dyes, anionic dyes and endocrine disruptors (nonionic pollutants) were tested. MV and CR were chosen as the adsorbates because MV could form cations and CR could form anions after they dissociated in water. Moreover, the pollutants with different solubilities were also chosen, including BPA and BP. The solubility of BPA and BP in water decreased orderly; they were dissolved in ethanol firstly, and then diluted in DI water. The removal ratios of the pollutants by PES/GO-0 and PES/GO-3 particles are shown in Fig. 9. It can be observed clearly that with the blending of GO, the removal ratios of MB and MV increased obviously, and yet the

Table 5
The maximal adsorbed amount of GO aqueous solution and GO in the particles.

GO situation	Aqueous solution	PES/GO-1	PES/GO-2	PES/GO-3	PES/GO-4
Adsorbed amount (mg/g)	1131.22	1010.00	724.67	694.44	505.09

amount of CR adsorbed was still quite low, which indicated that PES/GO particles had no adsorption capability on anionic reagents. The removal ratios of BPA and BP showed no difference between PES/GO-0 and PES/GO-3, and both of them were quite low, which indicated that the adsorption capability of PES/GO particles to the reagents with low solubility was not so significant, and the adsorbed amounts were caused by the hydrophobic interaction between the PES and reagents [23]. In general, the PES/GO particles had maintained the good selective adsorption capability for cationic compounds as GO.

4. Conclusion

In this work, PES enwrapped GO porous particles were successfully prepared by means of a liquid–liquid phase separation technique. The problems of recovery and control, which usually occurred when GO sheets were used as adsorbents in wastewater, were solved through this simple method. After introduction of small quantities of GO, the adsorption capability of the porous particles to MB was increased obviously. The adsorption process of MB was studied under various conditions including contacting times, initial concentrations, temperatures and pH values, and the data were used for the investigation of adsorption kinetics and adsorption isotherms. The adsorption process agreed with the pseudo-second-order model and fitted with Langmuir isotherm. The application of intraparticle diffusion model indicated that the adsorption process was controlled by the pore diffusion process. To further confirm the selective adsorption capacity of the particles, different pollutants were tested, including other dyes and endocrine disruptors, the results indicated that the PES/GO porous particles showed good selective adsorbability to cationic dyes. We anticipated that this method of preparing PES/GO particles could open up a route for the application of GO as adsorbent and made some potential contributions to the fields of waste water treatment.

Acknowledgements

This work was financially sponsored by the National Natural Science Foundation of China (Nos. 50973070, 51073105 and 51173119), State Education Ministry of China (Doctoral Program for High Education, No. 20100181110031), and Program for Changjiang Scholars and Innovative Research Team in University (IRT1163). We would like to thank our laboratory members for their generous help, and gratefully acknowledge the help of Ms. H. Wang of the Analytical and Testing Center at Sichuan University, for the SEM micrographs.

Appendix A. Supplementary material

The characterization of GO. The calculating method of porosity and pore volume of the particles. The application and discussion of pseudo-first-order kinetic model. The results and discussion of the adsorbed amount of MB on GO aqueous solution. Supplementary data associated with this article can be found, in the online version, at http://dx.doi.org/10.1016/j.cej.2012.11.009.

References

[1] M.S. Chiou, P.Y. Ho, H.Y. Li, Adsorption behavior of dye AAVN and RB4 in acid solutions on chemically cross-linked chitosan beads, J. Chin. Inst. Chem. Eng. 34 (2003) 625–634.
[2] Y.F. Lin, H.W. Chen, P.S. Chien, C.S. Chiou, C.C. Liu, Application of bifunctional magnetic adsorbent to adsorb metal cations and anionic dyes in aqueous solution, J. Hazard. Mater. 185 (2011) 1124–1130.
[3] M. Tekbaş, N. Bektaş, H.C. Yatmaz, Adsorption studies of aqueous basic dye solutions using sepiolite, Desalination 249 (2009) 205–211.
[4] M. Rafatullah, O. Sulaiman, R. Hashim, A. Ahmad, Adsorption of methylene blue on low-cost adsorbents: a review, J. Hazard. Mater. 177 (2010) 70–80.
[5] R.P.S. Suri, J.C. Crittenden, Removal and destruction of organic compounds in water using adsorption, steam regeneration, and photocatalytic oxidation processes, J. Environ. Eng. 125 (1999) 897–905.
[6] P.J. Cyr, R.P.S. Suri, E.D. Helmig, A pilot scale evaluation of removal of mercury from pharmaceutical wastewater using granular activated carbon, Water Res. 36 (2002) 4725–4734.
[7] J.H. Lee, D.I. Song, Y.W. Jeon, Adsorption of organic phenojs onto dual organic cation montmorillonite from water, Sep. Sci. Technol. 32 (1997) 1975–1992.
[8] N.F. Srasra, E. Srasra, Acid treatment of south Tunisian palygorskite: removal of Cd (II) from aqueous and phosphoric acid solutions, Desalination 250 (2010) 26–34.
[9] J. Pan, X. Zou, X. Wang, W. Guan, C. Li, Y. Yan, X. Wu, Adsorptive removal of 2,4-didichlorophenol and 2,6-didichlorophenol from aqueous solution by β-cyclodextrin/attapulgite composites: equilibrium, kinetics and thermodynamics, Chem. Eng. J. 166 (2011) 40–48.
[10] V. Vimonsesa, S. Lei, B. Jin, C.W.K. Chow, C. Saint, Kinetic study and equilibrium isotherm analysis of Congo Red adsorption by clay materials, Chem. Eng. J. 148 (2009) 354–364.
[11] B.O. Yoon, S. Koyanagi, T. Asano, M. Hara, A. Higuchi, Removal of endocrine disruptors by selective sorption method using polydimethylsiloxane membranes, J. Membr. Sci. 213 (2003) 137–144.
[12] L. Monser, N. Adhoum, Modified activated carbon for the removal of copper, zinc, chromium and cyanide from wastewater, Sep. Purif. Technol. 26 (2002) 137–146.
[13] B.H. Hameed, A.L. Ahmad, K.N.A. Latiff, Adsorption of basic dye (methylene blue) onto activated carbon prepared from rattan sawdust, Dyes Pigm. 75 (2007) 143–149.
[14] H. Jaegfeldt, T. Kuwana, G. Johansson, Electrochemical stability of catechols with a pyrene side chain strongly adsorbed on graphite electrodes for catalytic oxidation of dihydronicotinamide adenine dinucleotide, J. Am. Chem. Soc. 105 (1983) 1805–1814.
[15] X.K. Cheng, A.T. Kan, M.B. Tomson, Naphthalene adsorption and desorption from aqueous C_{60} fullerene, J. Chem. Eng. Data 49 (2004) 675–683.
[16] A. Stafiej, K. Pyrzynska, Adsorption of heavy metal ions with carbon nanotubes, Sep. Purif. Technol. 58 (2007) 49–52.
[17] F. Liu, S.Y. Chung, G. Oh, T. SeokSeo, Three-dimensional graphene oxide nanostructure for fast and efficient water-soluble dye removal, ACS Appl. Mat. Interfaces 4 (2012) 922–927.
[18] Y.J. Yao, S.D. Miao, S.M. Yu, L.P. Ma, H.Q. Sun, S.B. Wang, Fabrication of Fe_3O_4/SiO_2 core/shell nanoparticles attached to graphene oxide and its use as an adsorbent, J. Colloid Interface Sci. 379 (2012) 20–26.
[19] Y. Zhu, S. Murali, W. Cai, X. Li, J.W. Suk, J.R. Potts, R.S. Ruoff, Graphene and graphene oxide: synthesis, properties, and applications, Adv. Mater. 22 (2010) 3906–3924.
[20] W.J. Zhang, C.J. Zhou, W.C. Zhou, A.H. Lei, Q.L. Zhang, Q. Wan, B.S. Zou, Fast and considerable adsorption of methylene blue dye onto graphene oxide, Bull. Environ. Contam. Toxicol. 87 (2011) 86–90.
[21] S. Stankovich, R.D. Piner, X. Chen, N. Wu, S.T. Nguyen, R.S. Ruoff, Stable aqueous dispersions of graphitic nanoplatelets via the reduction of exfoliated graphite oxide in the presence of poly(sodium 4-styrenesulfonate), J. Mater. Chem. 16 (2006) 155–158.
[22] M.Z. Kassaee, E. Motamedi, M. Majdi, Magnetic Fe_3O_4–graphene oxide/polystyrene: fabrication and characterization of a promising nanocomposite, Chem. Eng. J. 172 (2011) 540–549.
[23] C.S. Zhao, Q.R. Wei, K.G. Yang, X.D. Liu, M. Nomizu, N. Nishi, Preparation of porous polysulfone beads for selective removal of endocrine disruptors, Sep. Purif. Technol. 40 (2004) 297–302.
[24] F.M. Cao, P.L. Bai, H.C. Li, Y.L. Ma, X.P. Deng, C.S. Zhao, Preparation of polyethersulfone–organophilic montmorillonite hybrid particles for the removal of bisphenol A, J. Hazard. Mater. 162 (2009) 791–798.
[25] S.D. Sun, J.Y. Hunag, C.S. Zhao, Polymeric particles for the removal of endocrine disruptors, Sep. Purif. Rev. 40 (2011) 312–337.
[26] H. Li, S. Pang, S. Wu, X. Feng, K. Müllen, C. Bubeck, Layer-by-layer assembly and UV photoreduction of graphene–polyoxometalate composite films for electronics, J. Am. Chem. Soc. 133 (2011) 9423–9429.
[27] A. Rodríguez, G. Ovejero, M. Mestanza, J. García, Removal of dyes from wastewaters by adsorption on sepiolite and pansil, Ind. Eng. Chem. Res. 49 (2010) 3207–3216.
[28] W. Zou, Y. Huang, J. Luo, J. Liu, C. Zhao, Poly (methyl methacrylate–acrylic acid–vinyl pyrrolidone) terpolymer modified polyethersulfone hollow fiber membrane with pH sensitivity and protein antifouling property, J. Membr. Sci. 358 (2010) 76–84.
[29] J.C. Wang, C.H. Xu, H.T. Hu, L. Wan, R. Chen, H. Zheng, F.M. Liu, M. Zhang, X.P. Shang, X.B. Wang, Synthesis, mechanical, and barrier properties of LDPE/graphene nanocomposites using vinyl triethoxysilane as a coupling agent, J. Nanopart. Res. 13 (2011) 869–878.
[30] S. Yang, X. Feng, S. Ivanovici, K. Müllen, Fabrication of graphene-encapsulated oxide nanoparticles: towards high-performance anode materials for lithium storage, Angew. Chem. Int. Edit. Engl. 49 (2010) 8408–8411.
[31] P. Bradder, S.K. Ling, S.B. Wang, S.M. Liu, Dye adsorption on layered graphite oxide, J. Chem. Eng. Data 56 (2010) 138–141.

[32] M.H. Min, L.D. Shen, G.S. Hong, M.F. Zhu, Y. Zhang, X.F. Wang, Y.M. Chen, B.S. Hsiao, Micro-nano structure poly (ether sulfones)/poly (ethyleneimine) nanofibrous affinity membranes for adsorption of anionic dyes and heavy metal ions in aqueous solution, Chem. Eng. J. 197 (2012) 88–100.
[33] M. Doğan, Y. Özdemir, M. Alkan, Adsorption kinetics and mechanism of cationic methyl violet and methylene blue dyes onto sepiolite, Dyes Pigm. 75 (2007) 701–713.
[34] S.S. Gupta, K.G. Bhattacharyya, Removal of Cd (II) from aqueous solution bykaolinite, montmorillonite and their poly (oxo zirconium) and tetrabutylam-monium derivatives, J. Hazard. Mater. B 128 (2006) 247–257.
[35] X. Yang, B. Al-Duri, Kinetic modelling of liquid-phase adsorption of reactive dyes on activated carbon, J. Colloid Interface Sci. 287 (2005) 25–34.
[36] F.C. Wu, R.L. Tseng, R.S. Juang, Initial behavior of intraparticle diffusion model used in the description of adsorption kinetics, Chem. Eng. J. 153 (2009) 1–8.
[37] C. Cheng, L. Ma, J. Ren, L.L. Li, G.F. Zhang, Q.G. Yang, C.S. Zhao, Preparation of polyethersulfone-modified sepiolite hybrid particles for the removal of environmental toxins, Chem. Eng. J. 171 (2011) 1132–1142.
[38] G. Crini, H.N. Peindy, F. Gimbert, C. Robert, Removal of CI basic green 4 (malachite green) from aqueous solutions by adsorption using cyclodextrin-based adsorbent: kinetic and equilibrium studies, Sep. Purif. Technol. 53 (2007) 97–110.
[39] E.N. Ei Qada, S.J. Allen, G.M. Walker, Adsorption of basic dyes from aqueous solution onto activated carbons, Chem. Eng. J. 135 (2008) 174–184.
[40] E.N. El Qada, S.J. Allen, G.M. Walker, Adsorption of methylene blue onto activated carbon produced from steam activated bituminous coal: a study of equilibrium adsorption isotherm, Chem. Eng. J. 124 (2006) 103–110.